

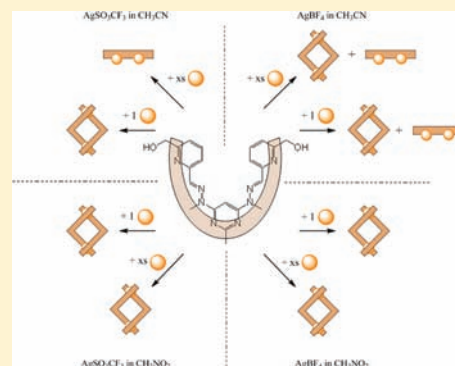
Sensitivity of Silver(I) Complexes of a Pyrimidine–Hydrazone Ligand to Solvent, Counteranion, and Metal-to-Ligand Ratio Changes

Daniel J. Hutchinson, Scott A. Cameron, Lyall R. Hanton,* and Stephen C. Moratti

Department of Chemistry, University of Otago, P.O. Box 56, Dunedin, New Zealand

Supporting Information

ABSTRACT: Metal complexation studies were performed with AgSO_3CF_3 and AgBF_4 and the ditopic pyrimidine–hydrazone ligand 6-(hydroxymethyl)pyridine-2-carboxaldehyde (2-methylpyrimidine-4,6-diyl)bis(1-methylhydrazone) (**1**) in both CH_3CN and CH_3NO_2 in a variety of metal-to-ligand ratios. The resulting complexes were studied in solution by NMR spectroscopy and in the solid state by X-ray crystallography. Reacting either AgSO_3CF_3 or AgBF_4 with **1** in either CH_3CN or CH_3NO_2 in a 1:1 metal-to-ligand ratio produced a double helicate in solution. This double helicate could be converted into a linear complex by increasing the metal-to-ligand ratio; however, the degree of conversion depended on the solvent and counteranion used. Attempts to crystallize the linear AgSO_3CF_3 complex resulted in crystals with the dimeric structure $[\text{Ag}_2\text{I}(\text{CH}_3\text{CN})_2]_2(\text{SO}_3\text{CF}_3)_4$ (**2**), while attempts to crystallize the AgSO_3CF_3 double helicate from CH_3CN resulted in crystals of another dimeric complex, $[\text{Ag}_2\text{I}(\text{SO}_3\text{CF}_3)(\text{CH}_3\text{CN})_2]_2(\text{SO}_3\text{CF}_3)_2 \cdot \text{H}_2\text{O}$ (**3**). The AgSO_3CF_3 double helicate was successfully crystallized from a mixture of CH_3CN and CH_3NO_2 and had the structure $[\text{Ag}_2\text{I}_2](\text{SO}_3\text{CF}_3)_2 \cdot 3\text{CH}_3\text{NO}_2$ (**4**). The linear AgBF_4 complex could not be isolated from the double helicate in solution; however, crystals grown from a solution containing both the AgBF_4 double helicate and linear complexes in CH_3CN had the structure $[\text{Ag}_2\text{I}(\text{CH}_3\text{CN})_2](\text{BF}_4)_2$ (**5**). The AgBF_4 double helicate could only be crystallized from CH_3NO_2 and had the structure $[\text{Ag}_2\text{I}_2](\text{BF}_4)_2 \cdot 2\text{CH}_3\text{NO}_2$ (**6**).



INTRODUCTION

Ag^{I} ions have a reputation in metallocsupramolecular chemistry for producing a wide variety of structures because of their d^{10} -electron configuration, resulting in a lack of stereochemical preference upon coordination to suitable donor atoms.^{1,2} In addition, weak interactions and crystal-packing forces tend to have a greater influence on the solid-state structure of silver(I) complexes,³ resulting in drastic changes in the supramolecular arrangement due to variations in the ligand composition,⁴ counteranion,⁵ and solvent choices⁶ and the metal-to-ligand ratios used.

It has been previously reported that the reaction between a ditopic pyrimidine–hydrazone (pym–hyz) ligand and AgBF_4 resulted in one of two different complex structures depending on the metal-to-ligand ratio used.⁷ When reacted in a 1:1 metal-to-ligand ratio, a double-helicate complex is produced in both solution and the solid state, as shown by NMR spectroscopy and X-ray crystallography. At this low metal-to-ligand ratio, the Ag^{I} ions do not bind to the pym N donors of the ligand and therefore do not induce the transoid-to-cisoid conformational change of the pym–hyz linkage.^{8,9} This is in contrast to metals such as Cu^{II} , Zn^{II} , and Pb^{II} , which do cause conformational change when reacted in 1:1 metal-to-ligand ratios, resulting in $[2 \times 2]$ grid structures.^{9,10} Conversion of this Ag^{I} double helicate to a linear complex, containing two Ag^{I} ions per ligand and cisoid pym–hyz bonds, occurs at higher metal-to-ligand ratios. The double helicate is remarkably stable in the presence

of unreacted Ag^{I} ; consequently, a 12:1 metal-to-ligand ratio is necessary for 85% conversion of the double helicate to the linear complex (Figure 1).⁷

Our ditopic pym–hyz ligand 6-(hydroxymethyl)pyridine-2-carboxaldehyde (2-methylpyrimidine-4,6-diyl)bis(1-methylhydrazone) (**1**) differs from those reported previously because of the addition of hydroxymethyl arms on the terminal pyridine (py) rings.¹¹ These arms have been included in order to incorporate the pym–hyz strand into larger chemical systems, where the conformational change expressed upon metal-ion coordination⁸ could be used to power useful devices such as polymer gel actuators, sensors, and artificial muscles.¹² However, these arms have been shown to exert control over the coordination chemistry of the pym–hyz strand because their positioning on the terminal py ring allows them to bind to the metal ion occupying the pym–hyz–py coordination sites. This binding prevents the formation of a $[2 \times 2]$ grid complex when Cu^{II} reacts with **1** in a 1:1 metal-to-ligand ratio, resulting in bent monocopper complexes.¹¹ Grid complexes are formed when **1** is reacted with Pb^{II} ions in a 1:1 metal-to-ligand ratio; because of the Pb^{II} ion's larger size, however binding of the hydroxymethyl arms does result in considerable distortion to the grid structure.¹³

Received: November 27, 2011

Published: April 11, 2012

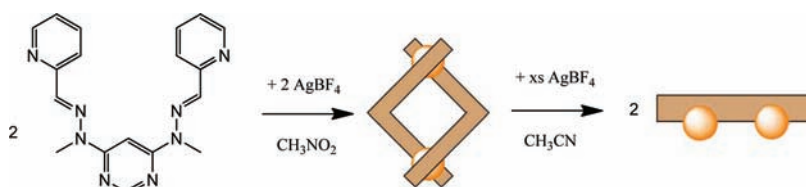


Figure 1. Reaction of a ditopic pym–hyz ligand strand with AgBF₄ results in a double helicate complex at a 1:1 metal-to-ligand ratio, which is then converted to a linear complex at higher metal-to-ligand ratios.⁷

It was hypothesized that, because of their large and flexible coordination spheres and their preference for N donors over O donors, Ag^I ions would only be affected to a small degree by the presence of the hydroxymethyl arms in ligand **1**. However, we report that the silver(I) chemistry of ligand **1** is much more complicated than that of previous pym–hyz ligands because the complexes formed in solution and the solid state were sensitive to the Ag^I counteranion (SO₃CF₃⁻ vs BF₄⁻) and solvent (CH₃CN vs CH₃NO₂) used, as well as the metal-to-ligand ratio. The structures of the complexes formed in solution were determined by NMR spectroscopy. Single crystals were also grown from the reaction solutions in order to determine, by X-ray crystallography, the solid-state structure of the complexes formed. The results showed that in most cases the solid-state structures of the complexes were significantly different from the structures present in solution.

EXPERIMENTAL SECTION

General Procedures. All chemicals were used as received without further purification. Ligand **1** was prepared according to the literature method.¹¹ AgSO₃CF₃ and AgBF₄ were acquired from Aldrich. All solvents were used as received and were of LR grade or better.

Microanalyses were carried out in the Campbell Microanalytical Laboratory, University of Otago, Dunedin, New Zealand. All measured microanalysis results had an uncertainty of ±0.4%. ¹H and ¹³C NMR spectra and two-dimensional (gCOSY, NOSEY, HSQC, and gHMBC) spectra were collected on a 500 MHz Varian UNITY INOVA spectrometer at 298 K. Spectra were collected in either CD₃CN or CD₃NO₂ and were referenced to the internal solvent signal, with chemical shifts reported in δ units (ppm). Electrospray mass spectrometry (ESMS) was carried out on a Bruker micro-TOFQ instrument (Bruker Daltronics, Bremen, Germany). Samples were introduced using direct infusion into an electrospray ionization source in positive mode. Sampling was averaged for 2 min over a range of *m/z* 50–3000 amu. The mass was calibrated using an external calibrant of sodium formate clusters, with 15 calibration points from 90 to 1050 amu, using a quadratic plus HPC line fit. ESMS spectra were processed using *Compass* software (version 1.3; Bruker Daltronics, Bremen, Germany). IR spectra were recorded on a Bruker Alpha-P ATR-IR spectrometer.

Ag₂1(SO₃CF₃)₂. AgSO₃CF₃ (93.5 mg, 0.366 mmol) in CH₃CN (15 mL) was added to **1** (30.5 mg, 0.073 mmol), which gave a yellow solution with agitation at room temperature. A yellow solid was precipitated from the solution by the addition of diethyl ether (23.3 mg, 34%). Anal. Calcd for C₂₃H₂₄N₈O₈S₂F₆Ag₂·H₂O: C, 29.01; H, 2.75; N, 11.77. Found: C, 28.86; H, 2.67; N, 11.55. ¹H NMR (500 MHz, CD₃CN): δ 8.00 (2H, s, H9), 7.97 (2H, t, J = 7.7 Hz, H12), 7.69 (2H, d, J = 7.7 Hz, H13), 7.51 (2H, d, J = 7.6 Hz, H11), 6.51 (1H, s, H5), 4.87 (4H, d, J = 5.8 Hz, H15), 4.05 (2H, t, J = 5.8 Hz, H16), 3.60 (6H, s, H8), 2.85 (3H, s, H7). ¹³C NMR (500 MHz, CD₃CN): δ 168.05 (C2), 163.28 (C14), 161.18 (C4,6), 149.66 (C10), 140.09 (C10), 136.93 (C9), 125.77 (C11), 123.22 (C15), 86.84 (C5), 65.61 (C15), 33.81 (C8), 28.64 (C7). ESMS. Calcd for C₂₁H₂₄N₈O₂Ag⁺: *m/z* 527.10677. Found: *m/z* 527.12668. Selected IR (cm⁻¹): ν 3417 (s, br, OH str), 2931 (m, CH str), 1591 (s), 1551 (s, C=N str), 1486 (s), 1353 (w), 1254 (s, br, SO₃CF₃⁻), 1155 (s), 1032 (s), 984 (s). Yellow crystals suitable for X-ray determination

were grown by the slow diffusion of diethyl ether into a CH₃CN solution of Ag₂1(SO₃CF₃)₂. These crystals gave the structure [Ag₂1(CH₃CN)₂]₂(SO₃CF₃)₄ (**2**).

Ag₂1₂(SO₃CF₃)₂. AgSO₃CF₃ (27.8 mg, 0.102 mmol) in CH₃CN (6 mL) was added dropwise to a suspension of **1** (45.2 mg, 0.106 mmol) in CH₃CN (4 mL) with stirring at 80 °C. This resulted in partial dissolution of **1** and the formation of a yellow solution. This mixture was filtered, and diethyl ether was added to the yellow filtrate, causing precipitation of an off-white solid. This solid was washed with diethyl ether and dried in vacuo (21.2 mg, 32%): Anal. Calcd for C₂₂H₂₄N₈O₅SF₃Ag₂·H₂O: C, 38.00; H, 3.77; N, 16.11. Found: C, 38.04; H, 3.53; N, 15.85. ¹H NMR (500 MHz, CD₃CN): δ 7.97 (2H, t, J = 7.7 Hz, H12), 7.94 (2H, s, H9), 7.60 (2H, d, J = 7.5 Hz, H11), 7.30 (2H, d, J = 7.8 Hz, H13), 7.16 (1H, s, H5), 4.00 (2H, dd, J = 5.1 and 14.9 Hz, H15a) 3.89 (2H, dd, J = 5.7 and 14.8 Hz, H15b), 3.59 (2H, t, J = 5.5 Hz, H16), 3.32 (6H, s, H8), 2.26 (3H, s, H7). ¹³C NMR (500 MHz, CD₃CN): δ 166.91 (C2), 162.88 (C4, C6), 161.59 (C14), 150.80 (C10), 140.55 (C12), 138.89 (C9), 125.51 (C11), 123.71 (C13), 89.57 (C5), 64.83 (C15), 32.25 (C8), 25.89 (C7). ESMS. Calcd for (C₂₁H₂₄N₈O₂)₂Ag⁺: *m/z* 949.3251. Calcd for C₂₁H₂₄N₈O₂Ag⁺: *m/z* 527.1068. Calcd for C₂₁H₂₅N₈O₂⁺: *m/z* 421.2100. Found: *m/z* 949.2978, 527.1033, 421.2061. Selected IR (cm⁻¹): ν 3375 (w, OH str), 2925 (w, CH str), 1575 (s), 1544 (s, C=N str), 1482 (s), 1458 (m), 1446 (m), 1407 (s), 1282 (s), 1245 (s, br, SO₃CF₃⁻), 1222 (s), 1154 (s), 1095 (s), 1043 (s), 1026 (s). Yellow crystals suitable for X-ray determination were grown by the slow diffusion of diethyl ether into a CH₃CN solution of Ag₂1₂(SO₃CF₃)₂. These crystals gave the structure [Ag₂1(SO₃CF₃)(CH₃CN)₂]₂(SO₃CF₃)₂·H₂O (**3**).

The reaction was repeated in CH₃NO₂, with AgSO₃CF₃ (22.0 mg, 0.086 mmol) in CH₃NO₂ (5 mL) added dropwise to a suspension of **1** (35.8 mg, 0.085 mmol) with stirring in CH₃NO₂ (10 mL) at 100 °C. This resulted in a yellow solution, followed by precipitation of a yellow solid. The solid was filtered, washed with diethyl ether, and dried in vacuo (5.2 mg, 9%). ¹H NMR (500 MHz, DMSO-*d*₆): δ 8.10 (2H, s, H9), 8.07 (2H, t, J = 7.8 Hz, H12), 7.69 (2H, d, J = 7.6 Hz, H11), 7.36 (2H, d, J = 7.8 Hz, H13), 7.07 (1H, s, H5), 5.63 (2H, t, J = 5.2 Hz, H16), 3.91 (2H, dd, J = 5.1 and 14.9 Hz, H15a), 3.77 (2H, dd, J = 5.1 and 14.8 Hz, H15b), 3.29 (6H, s, H8), 2.22 (3H, s, H7). ESMS. Found: *m/z* 949.2994, 527.1054, 421.2072. Calcd for (C₂₁H₂₄N₈O₂)₂Ag⁺: *m/z* 949.3251. Calcd for C₂₁H₂₄N₈O₂Ag⁺: *m/z* 527.1068. Calcd for C₂₁H₂₅N₈O₂⁺: *m/z* 421.2100. Selected IR (cm⁻¹): ν 3408 (w, OH str), 1590 (w), 1547 (s, C=N str), 1455 (w), 1432 (w), 1409 (w), 1385 (w), 1274 (s), 1243 (s, br, SO₃CF₃⁻), 1225 (s), 1153 (s), 1026 (s).

The reaction was repeated in a mixture of CH₃CN and CH₃NO₂, with AgSO₃CF₃ (28.7 mg, 0.112 mmol) in CH₃CN (5 mL) added dropwise to a suspension of **1** (46.8 mg, 0.111 mmol) with stirring in CH₃NO₂ (10 mL) at 100 °C. This resulted in a yellow solution. Yellow crystals suitable for X-ray determination were grown by the slow diffusion of diethyl ether into this solution. These crystals gave the structure [Ag₂1₂](SO₃CF₃)₂·3CH₃NO₂ (**4**).

Ag₂1₂(BF₄)₂. Ag₂1₂(BF₄)₂ was prepared as described for Ag₂1₂(SO₃CF₃)₂ but with AgBF₄ (65.13 mg, 0.336 mmol) in CH₃CN (3 mL) and **1** (36.2 mg, 0.086 mmol) in CH₃CN (10 mL), which resulted in full dissolution of **1** and the formation of a yellow solution. Diethyl ether was added to cause precipitation of an off-white solid, which was washed with diethyl ether and EtOH and dried in vacuo (37.8 mg, 71%). Anal. Calcd for

Table 1

	[Ag ₂ I(CH ₃ CN) ₂] ₂ (SO ₃ CF ₃) ₄ (2)	[Ag ₂ I(SO ₃ CF ₃)(CH ₃ CN) ₂] ₂ (SO ₃ CF ₃) ₂ ·H ₂ O (3)	[Ag ₂ I ₂](SO ₃ CF ₃) ₂ ·3CH ₃ NO ₂ (4)
empirical formula	C ₅₄ H ₆₀ Ag ₄ F ₁₂ N ₂₀ O ₁₆ S ₄	C ₅₄ H ₆₀ Ag ₄ F ₁₂ N ₂₀ O ₁₇ S ₄	C ₄₆ H ₅₇ Ag ₂ F ₃ N ₁₉ O ₁₃ S
fw	2032.94	2048.94	1388.92
cryst syst	triclinic	monoclinic	orthorhombic
space group	<i>P</i> $\bar{1}$	<i>C2/c</i>	<i>Pbcn</i>
<i>a</i> /Å	8.8339(8)	21.065(4)	14.5504(5)
<i>b</i> /Å	12.8072(10)	27.459(5)	29.2736(9)
<i>c</i> /Å	15.3793(12)	15.881(3)	25.1803(7)
α /deg	97.165(4)	90	90
β /deg	92.266(4)	127.895(6)	90
γ /deg	95.012(4)	90	90
<i>V</i> /Å ³	1717.6(2)	7249(2)	10725.4(6)
<i>Z</i>	1	4	8
<i>T</i> /K	90(2)	90(2)	90(2)
μ /mm ⁻¹	1.360	1.291	0.863
reflns collected	34168	43788	100846
unique reflns (<i>R</i> _{int})	6368 (0.0337)	6732 (0.0332)	7148 (0.0540)
<i>R</i> 1 indices [<i>I</i> > 2 σ (<i>I</i>)]	0.0261	0.0782	0.0552
w <i>R</i> 2 (all data)	0.0663	0.2127	0.1240
GOF	1.082	1.056	1.083
	[Ag ₂ I(CH ₃ CN) ₂](BF ₄) ₂ (5)	[Ag ₂ I ₂](BF ₄) ₂ ·2CH ₃ NO ₂ (6)	
empirical formula	C ₂₅ H ₃₀ Ag ₂ B ₂ F ₈ N ₁₀ O ₂	C ₄₄ H ₅₄ Ag ₂ B ₂ F ₈ N ₁₈ O ₈	
fw	891.95	1321.89	
cryst syst	triclinic	monoclinic	
space group	<i>P</i> 1	<i>P2</i> ₁ / <i>n</i>	
<i>a</i> /Å	7.9175(15)	15.7298(17)	
<i>b</i> /Å	8.3277(18)	14.6064(13)	
<i>c</i> /Å	12.571(3)	22.919(2)	
α /deg	80.108(7)	90	
β /deg	77.305(7)	95.295(4)	
γ /deg	77.748(7)	90	
<i>V</i> /Å ³	783.3(3)	5240.3(9)	
<i>Z</i>	1	4	
<i>T</i> /K	90(2)	90(2)	
μ /mm ⁻¹	1.342	0.843	
reflns collected	8503	42319	
unique reflns (<i>R</i> _{int})	3182 (0.0257)	8030 (0.0346)	
<i>R</i> 1 indices [<i>I</i> > 2 σ (<i>I</i>)]	0.0481	0.0479	
w <i>R</i> 2 (all data)	0.1268	0.1310	
GOF	1.142	1.045	

C₂₁H₂₄N₈O₂AgBF₄·H₂O: C, 39.84; H, 4.14; N, 17.70. Found: C, 39.80; H, 4.05; N, 17.93. ¹H NMR (500 MHz, CD₃CN): δ 7.98 (2H, t, *J* = 7.8 Hz, H12), 7.94 (2H, s, H9), 7.60 (2H, d, *J* = 7.6 Hz, H11), 7.30 (2H, d, *J* = 7.8 Hz, H12), 7.16 (1H, s, H5), 4.00 (2H, dd, *J* = 5.2 and 14.9 Hz, H15a), 3.89 (2H, dd, *J* = 5.6 and 14.9 Hz, H15b), 3.49 (2H, t, *J* = 5.4 Hz, H16), 3.32 (6H, s, H8), 2.26 (3H, s, H7). ESMS. Calcd for C₂₁H₂₄N₈O₂Ag⁺: *m/z* 527.1068. Found: *m/z* 527.1031. Selected IR (cm⁻¹): ν 3522 (w, OH str), 2917 (w, CH str), 1574 (s), 1545 (s, C=N str), 1482 (s), 1459 (m), 1445 (m), 1406 (s), 1288 (w), 1226 (w), 1158 (s), 1039 (s, br, BF₄⁻). Yellow crystals suitable for X-ray determination were grown by the slow diffusion of diethyl ether into a CH₃CN solution of Ag₂I₂(BF₄)₂. These crystals gave the structure [Ag₂I(CH₃CN)₂](BF₄)₂ (5).

The reaction was repeated in CH₃NO₂, with AgBF₄ (30.1 mg, 0.16 mmol) in CH₃NO₂ (8 mL) added dropwise to a suspension of 1 (65.1 mg, 0.16 mmol) with stirring in CH₃NO₂ (5 mL) at 100 °C. This resulted in a yellow solution. Diethyl ether was added to precipitate an off-white solid, which was washed with diethyl ether and dried in vacuo (40.5 mg, 42%). Anal. Calcd for C₂₁H₂₄N₈O₂AgBF₄·1/2H₂O: C, 40.41; H, 4.04; N, 17.95. Found: C, 40.52; H, 4.24; N, 18.14. ¹H NMR (500 MHz, CD₃NO₂): δ 8.07 (2H, t, *J* = 7.6 Hz, H12), 8.06 (2H, s, H9), 7.68 (2H, d, *J* = 7.6 Hz, H11), 7.42 (2H, d, *J* = 7.7 Hz, H13), 7.35

(1H, s, H5), 4.17 (2H, d, *J* = 14.6 Hz, H15a), 4.08 (2H, d, *J* = 14.5 Hz, H15b), 3.43 (6H, s, H8), 2.31 (3H, s, H7). ESMS. Calcd for C₂₁H₂₄N₈O₂Ag⁺: *m/z* 527.1068. Found: *m/z* 527.1049. Selected IR (cm⁻¹): ν 3511 (w, OH str), 1604 (m), 1574 (m, C=N str), 1543 (m), 1481 (m), 1458 (m), 1399 (m), 1287 (m), 1223 (m), 1157 (m), 1033 (s). Yellow crystals suitable for X-ray determination were grown by the slow diffusion of diethyl ether into a CH₃NO₂ solution of Ag₂I₂(BF₄)₂. These crystals gave the structure [Ag₂I₂](BF₄)₂·2CH₃NO₂ (6).

X-ray Crystallography. Crystallographic data are summarized in Table 1. X-ray diffraction data were collected on a Bruker APEX II CCD diffractometer, with graphite-monochromated Mo *K* α (λ = 0.71073 Å) radiation. Intensities were corrected for Lorentz polarization effects,¹⁴ and a multiscan absorption correction¹⁵ was applied. The structures were solved by direct methods (SHELXS¹⁶ or SIR-97¹⁷) and refined on *F*² using all data by full-matrix least-squares procedures (SHELXL 97¹⁸). All calculations were performed using the WinGX interface.¹⁹ Detailed analyses of the extended structure were carried out using PLATON²⁰ and MERCURY²¹ (version 2.4).

Some of the crystal structures contained disordered components. The SO₃CF₃⁻ anions in 3 showed translational disorder over two sites with site occupancy factors of 0.67 and 0.33 and of 0.71 and 0.29,

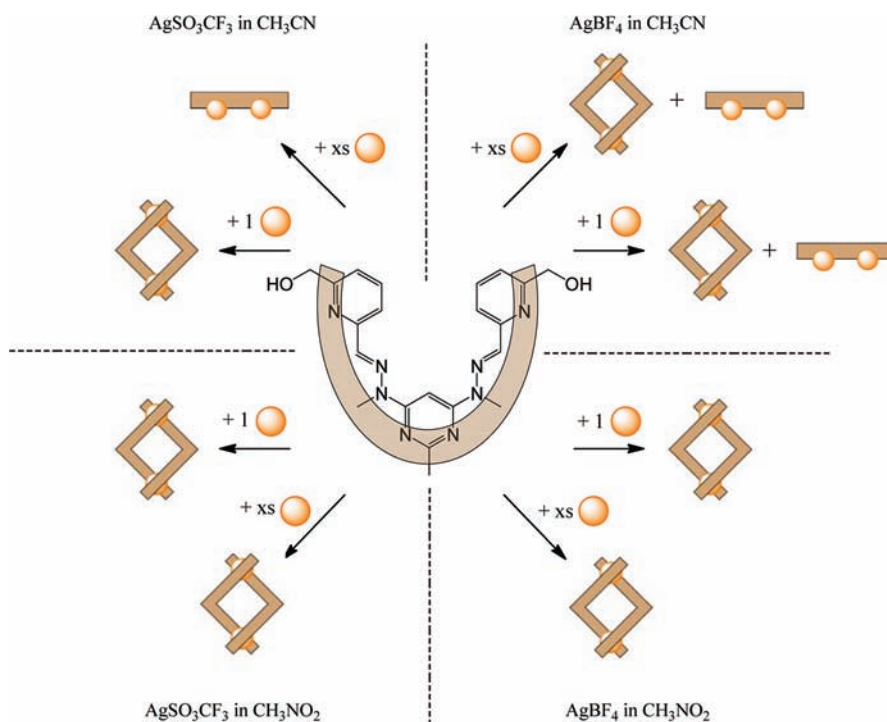


Figure 2. Schematic summarizing the complexes identified in solution by NMR studies when ligand **1** was reacted with either AgSO_3CF_3 (left) or AgBF_4 (right) in either CH_3CN (top) or CH_3NO_2 (bottom) on either a 1:1 or excess:1 metal-to-ligand ratio.

respectively. The bond lengths and angles on these SO_3CF_3^- anions had to be fixed because of their disorder. A total of 358 restraints were used to model the disordered SO_3CF_3^- anions. The H atoms of the H_2O molecule of crystallization in **3** could not be located. The hydroxymethyl arms containing O2 and O3 were disordered over two sites in **4** with site occupancy factors of 0.67 and 0.33 and of 0.74 and 0.26, respectively. Both SO_3CF_3^- counterions in **4** were also disordered.

The structure for **5** was racemically twinned and was refined accordingly.²² Two different data sets for **5** were collected and solved, both of which were of poor quality because of weak diffracting crystals. The solution reported herein represents the best quality solution.

The hydroxymethyl arm containing O2 in **6** was disordered over two sites with site occupancy factors of 0.54 and 0.46. One of the Ag^+ ions in **6** was also disordered over two sites, with site occupancy factors of 0.80 and 0.20. The crystals of complex **6** were also of poor quality, but as with complex **5**, their diffraction pattern allowed for the unambiguous description of the complex structure.

RESULTS AND DISCUSSION

Synthesis and Structures of Complexes. Ligand **1** was reacted with either AgSO_3CF_3 or AgBF_4 in either CH_3CN or CH_3NO_2 in various metal-to-ligand ratios. The reactions were repeated in either CD_3CN or CD_3NO_2 so the constitutions of the reaction solutions could be identified by NMR spectroscopy. Diethyl ether was then either added directly or added through slow diffusion into the reaction solutions to yield either powdered precipitates or crystalline samples of the complexes. It was found that, in solution, the primary structure of the complexes formed depended on three factors: (i) the metal-to-ligand ratio used; (ii) the counteranion of the metal salt used (SO_3CF_3^- or BF_4^-); and (iii) the solvent used (CH_3CN or CH_3NO_2 ; Figure 2).

Complexes Formed from AgSO_3CF_3 and **1.** Reacting AgSO_3CF_3 with **1** in CH_3CN in a 1:1 metal-to-ligand ratio exclusively formed a double-helicate complex in solution, as evidenced by NMR spectroscopy. The diffusion of diethyl ether

into the solution of this complex resulted in a yellow solid, which produced a microanalytical result consistent with the formula $\text{Ag}_2\text{SO}_3\text{CF}_3$. The slow diffusion of diethyl ether yielded small crystals, the structure of which was not a double helicate but instead the distorted 2:1 metal-to-ligand dimer **3**. These crystals were only characterized by X-ray diffraction because of the very small quantity produced.

When the 1:1 reaction between AgSO_3CF_3 and **1** was repeated in CH_3NO_2 , precipitation of a solid followed shortly after dissolution and complexation of **1**. NMR studies of this solid in dimethyl sulfoxide ($\text{DMSO}-d_6$) revealed that it was a mixture of the double-helicate complex identified in the previous CH_3CN reaction, as well as unreacted **1**. Repeating the reaction in a mixture of CH_3CN and CH_3NO_2 (1:2, by volume), however, resulted in complete dissolution and complexation of **1** without any subsequent precipitation. The slow diffusion of diethyl ether into this solution yielded crystals, the structure of which was the double helicate **4**.

When AgSO_3CF_3 was reacted with **1** in a 2:1 metal-to-ligand ratio in CH_3CN , a mixture of a 2:1 linear complex and the 1:1 double helicate was formed in solution, as evidenced by NMR studies. A metal-to-ligand ratio of 7:1 was necessary to produce a solution containing exclusively the 2:1 linear complex. Diffusion of diethyl ether into this solution produced a yellow solid, the microanalysis results of which were consistent with the formula $\text{Ag}_2\text{1}(\text{SO}_3\text{CF}_3)_2 \cdot \text{H}_2\text{O}$. Slow diffusion resulted in crystals of **2**. The linear 2:1 complex could not be formed in CH_3NO_2 . A yellow solution would form upon mixing AgSO_3CF_3 and **1** in CH_3NO_2 , after which a solid would precipitate. Even when a metal-to-ligand ratio of 8:1 was used, there was no evidence of the formation of any complex other than the 1:1 double helicate in either the precipitate or the solution phase of this mixture.

Complexes Formed from AgBF_4 and **1.** A metal-to-ligand ratio of 4:1 was necessary for complete complexation of

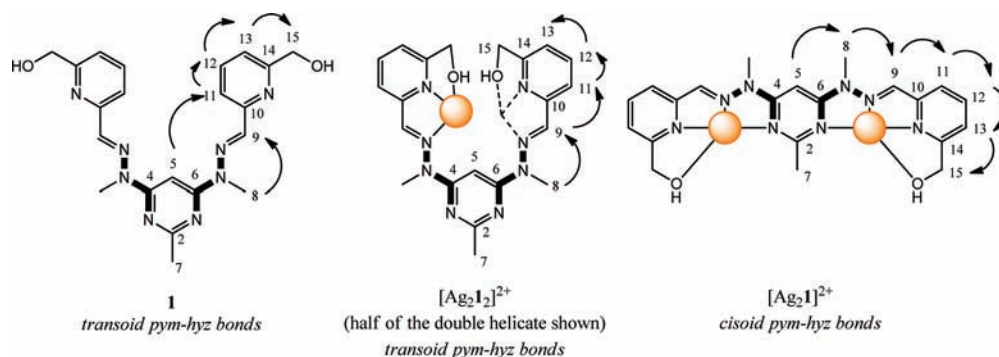


Figure 3. (left) NOE correlations of the free ligand **1**, which demonstrate its horseshoe shape.¹¹ (center) NOE correlations of the $[\text{Ag}_2\text{I}_2]^{2+}$ cation, common to the 1:1 metal-to-ligand complexes $\text{Ag}_2\text{I}_2(\text{SO}_3\text{CF}_3)_2$ and $\text{Ag}_2\text{I}_2(\text{BF}_4)_2$ identified in both CD_3CN and CD_3NO_2 (only half the double helicate is shown for clarity). (right) NOE correlations of the $[\text{Ag}_2\text{I}]^{2+}$ cation, common to the 2:1 metal-to-ligand linear complexes $\text{Ag}_2\text{I}(\text{SO}_3\text{CF}_3)_2$ and $\text{Ag}_2\text{I}_2(\text{BF}_4)_2$ identified in both CD_3CN and CD_3NO_2 (pym–hyz bonds are highlighted; showing NMR numbering).

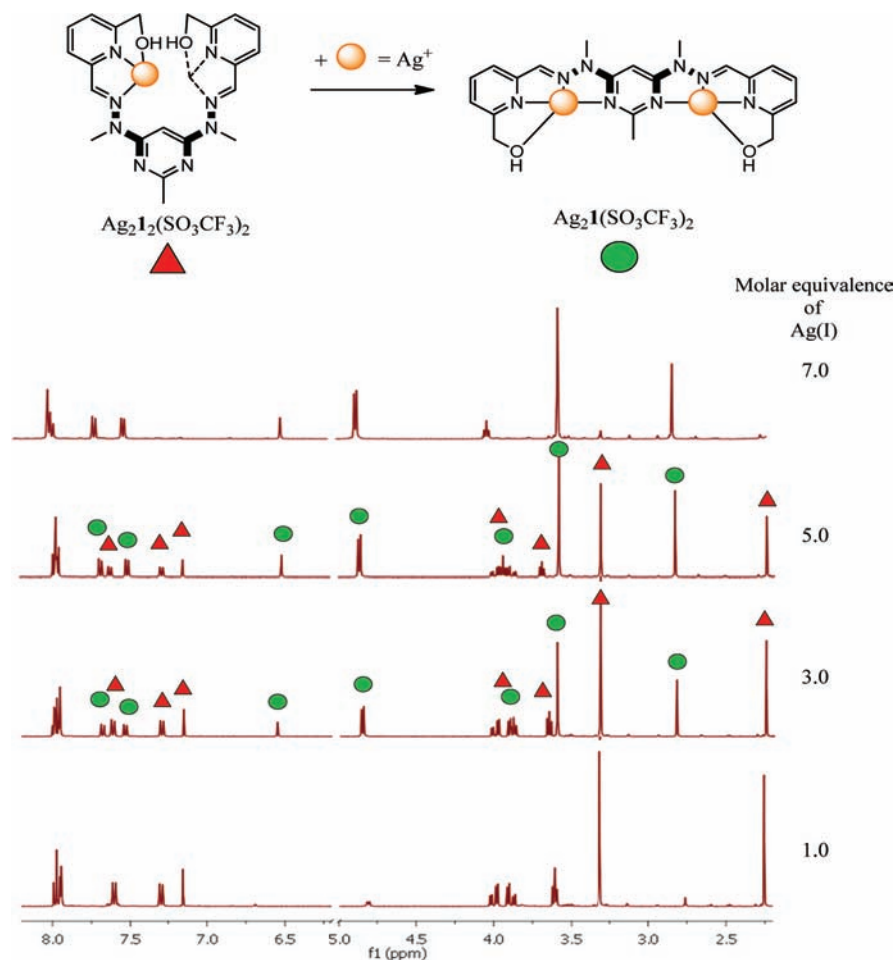


Figure 4. ^1H NMR spectra of the **1** and AgSO_3CF_3 reactions performed in CD_3CN , using metal-to-ligand ratios from 1:1 (bottom) to 7:1 (top).

1 with AgBF_4 in CH_3CN . This resulted in a solution containing the 1:1 double helicate with a small amount of a 2:1 linear complex as a minor product. Regardless of the metal-to-ligand ratio used, the ratio of these two complexes in solution was always 5:1, as evidenced by ^1H NMR spectroscopy. The direct addition of diethyl ether to this solution produced a yellow solid, which was consistent with the formula $\text{Ag1BF}_4\cdot\text{H}_2\text{O}$, as evidenced by microanalysis. The slow diffusion of diethyl ether produced very small crystals, which had the structure **5**, which was consistent with a 2:1 linear complex, not a 1:1 double

helicate. Unfortunately, there was not enough crystalline material produced for analysis by any means other than X-ray diffraction.

AgBF_4 was also reacted with **1** in CH_3NO_2 in a 1:1 metal-to-ligand ratio, resulting in complete dissolution and complexation of **1**. NMR studies confirmed that the complex in solution was a 1:1 double helicate, identical with the complex identified when AgBF_4 and **1** were reacted in CH_3CN . The direct addition of diethyl ether resulted in a yellow solid, consistent with the formula $\text{Ag1BF}_4\cdot\frac{1}{2}\text{H}_2\text{O}$, as shown by microanalysis.

The slow diffusion of diethyl ether resulted in crystals of a double-helicate complex **6**. AgBF_4 and **1** were also reacted in metal-to-ligand ratios of up to 8:1 in CH_3NO_2 . NMR studies showed that these solutions contained only the 1:1 double-helicate complex.

NMR Spectroscopy. The ^1H NMR spectra from the solution of the 1:1 AgSO_3CF_3 and **1** reactions in CH_3CN and CH_3NO_2 indicated that the complex in solution was a double helicate, consisting of two molecules of **1** sharing two Ag^{I} ions. The ^1H NMR spectra showed only nine peaks, indicating that the complex was symmetrical, with a Ag^{I} ion bound in each of the pym-hyz coordination pockets. Nuclear Overhauser enhancement (NOE) correlations were observed among H8_{hyz} , H9_{hyz} , and H11_{py} but not between H5_{pym} and H8_{hyz} (Figure 3). This indicated two details about the double helicate's structure: (i) that the pym-hyz bonds were transoid, as seen in the free ligand **1**,¹¹ and (ii) that the py ring in the 1:1 AgSO_3CF_3 and **1** complex was rotated such that the py N atom faced toward the center of the complex. Rotation of the hydroxymethyl arms was restricted because of coordination of the OH groups to the Ag^{I} ions. This was evidenced in the ^1H NMR spectrum by the H15 methylene protons occupying different chemical environments and therefore exhibiting two signals with different chemical shifts, which showed geminal coupling (Figure 4). The transoid shape of the pym-hyz bonds and the binding of the OH groups to the Ag^{I} ions rule out the possibility that the 1:1 metal-to-ligand complex existed as any other kind of coordination isomer other than a double helicate.

Increasing the AgSO_3CF_3 -to-**1** ratio from 1:1 to 7:1 in CH_3CN resulted in the conversion of the double helicate to a 2:1 linear complex (Figure 4). The ^1H NMR spectrum of this linear complex showed only nine peaks and exhibited NOE correlations between H5_{pym} , H8_{hyz} , H9_{hyz} , and H11_{py} . This indicated a symmetrical, linear shape, with a Ag^{I} ion in each coordination pocket. The H15 methylene proton signal in the spectrum of the linear complex did not express geminal coupling, for although the binding of the hydroxymethyl arm to the Ag^{I} ions would prevent rotation of the arm, the chemical shifts of the methylene proton positions were coincidentally the same. The chemical shift of the methylene signals for the linear complex was 4.87 ppm, compared to 4.00 and 3.89 ppm for these signals in the double helicate, as a result of the hydroxymethyl arms of the 1:1 complex being shielded by the double-helicate shape. Another major difference was the chemical shift of the H5_{pym} signal. In the spectrum of the linear complex, this signal was located at 6.51 ppm, similar to previously reported linear lead(II) and zinc(II) complexes of **1**.¹³ The H5_{pym} peak in the spectrum of the double helicate was located at 7.16 ppm, which was closer in chemical shift to the H5_{pym} signal of the free ligand at 7.65 ppm.¹¹ The difference in the chemical shift of H5_{pym} appears to be due to the conformation of the pym-hyz linkages.

When the reaction between AgSO_3CF_3 and **1** was repeated in CH_3NO_2 , a solid would precipitate from the reaction mixture shortly after mixing. This solid proved insoluble in CD_3NO_2 ; however, it was dissolved in $\text{DMSO}-d_6$ to give a ^1H NMR spectrum. Regardless of the metal-to-ligand ratio used in the reaction, the spectrum obtained from the solid precipitate was always very similar to that of the $\text{Ag}_2\text{I}_2(\text{SO}_3\text{CF}_3)_2$ complex synthesized in CD_3CN . The spectra all showed nine peaks, with chemical shifts very similar to those seen in the spectra of the $\text{Ag}_2\text{I}_2(\text{SO}_3\text{CF}_3)_2$ complex in CD_3CN . The H15 methylene proton signals showed geminal coupling. This indicated that

the double-helicate $\text{Ag}_2\text{I}_2(\text{SO}_3\text{CF}_3)_2$ complex was formed in CH_3NO_2 as well as in CH_3CN .

The ^1H NMR spectra of the reaction solutions, formed by reacting AgBF_4 with **1** in CD_3CN in various metal-to-ligand ratios, all showed a mixture of a $\text{Ag}_2\text{I}_2(\text{BF}_4)_2$ double helicate and a $\text{Ag}_2\text{I}(\text{BF}_4)_2$ linear complex in roughly a 5:1 ratio. The spectra from both of these complexes were virtually identical with those of their SO_3CF_3^- counterparts, with the only differences being minor chemical shifts for the hydroxymethyl proton signals.

The spectrum of the AgBF_4 and **1** 1:1 reaction mixture in CD_3NO_2 was consistent with the formation of a $\text{Ag}_2\text{I}_2(\text{BF}_4)_2$ double helicate. Nine peaks were present, indicating a symmetrical molecule. The H15 methylene proton signals expressed geminal coupling, and the H5_{pym} signal was located at 7.35 ppm. Even when the metal-to-ligand ratio was increased to 4:1, there were no signals due to a $\text{Ag}_2\text{I}(\text{BF}_4)_2$ complex detected.

IR Spectroscopy. The linear and double-helicate AgSO_3CF_3 complexes displayed OH stretching bands at 3417 and 3397 cm^{-1} , respectively. The linear AgSO_3CF_3 complex's IR spectrum contained an intense band at 1591 cm^{-1} , in addition to the C=N stretching mode at 1551 cm^{-1} , while the double-helicate spectrum displayed a much weaker band at 1576 cm^{-1} . The difference in intensity between the C=N stretching mode and the bands from 1455 to 1385 cm^{-1} was much greater for the double helicate.

The solids obtained by the diffusion of diethyl ether into CH_3CN solutions of AgBF_4 and **1** of various metal-to-ligand ratios all showed identical IR spectra. These spectra contained a C=N stretching mode at 1545 cm^{-1} , as well as an intense band at 1039 cm^{-1} due to vibrations of the BF_4^- counterions. Likewise, the IR spectra of the products from the CH_3NO_2 solutions of AgBF_4 and **1** were the same regardless of the metal-to-ligand ratio. The C=N stretching modes in these spectra were located at 1543 cm^{-1} .

X-ray Crystallography. X-ray-quality single crystals were grown by the slow diffusion of diethyl ether into reaction solutions of AgSO_3CF_3 or AgBF_4 and **1** in CH_3CN or CH_3NO_2 . The resulting crystal structures were often at odds with the structures of the complexes identified in solution, by NMR spectroscopy, and the composition of the powders precipitated by the direct addition of diethyl ether, as determined by microanalysis.

X-ray Crystal Structure of 2. Crystals of complex **2** were obtained by the slow addition of diethyl ether into a CH_3CN solution containing AgSO_3CF_3 and **1** in a 5:1 metal-to-ligand ratio. Complex **2** crystallized in the triclinic space group $P\bar{1}$, with one $[\text{Ag}_2\text{I}(\text{CH}_3\text{CN})_2]^{2+}$ cation and two SO_3CF_3^- anions in the asymmetric unit (Figure 5). The complex had a stretched-out linear shape, with a centroid-centroid distance between the py rings of 13.98 Å. Both coordination pockets contained a Ag^{I} ion. Ag^{I} existed in a distorted trigonal-bipyramidal environment, with a τ_5 parameter equal to 0.66.²³ Ag^{I} was bound to all three of the N donors of one pym-hyz-py coordination site, a CH_3CN molecule, and the hydroxymethyl donor O1A on a symmetry-generated $[\text{Ag}_2\text{I}(\text{CH}_3\text{CN})_2]^{2+}$ cation. This $\text{Ag}^{\text{I}}-\text{O1A}$ bond was a formal coordination bond, with a distance of 2.693(3) Å. Consequently, complex **2** existed as an offset, parallel, centrosymmetric dimer (Figure 6). The geometry around Ag^{II} was a relatively rare distorted square plane^{1,24} with a τ_4 parameter equal to 0.36²⁵ (Figure 5).

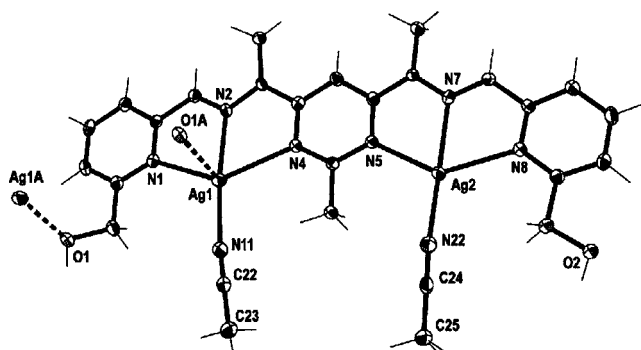


Figure 5. View of one of the $[\text{Ag}_2\text{I}(\text{CH}_3\text{CN})_2]^{2+}$ cations that made up the dimer of complex 2 (crystallographic numbering). Thermal ellipsoids drawn at the 50% probability level (symmetry code: A, $2 - x, 2 - y, 1 - z$).

The dimers were arranged so that the $[\text{Ag}_2\text{I}(\text{CH}_3\text{CN})_2]^{2+}$ cations faced each other, with the pym methyl groups pointing in opposite directions. The unbound SO_3CF_3^- counterions were connected to the dimer via hydrogen bonds, with lengths of 2.01(4) and 1.90(4) Å for $\text{O1-H}\cdots\text{O12}$ and $\text{O2-H}\cdots\text{O23}$, respectively [corresponding to $\text{O1}\cdots\text{O12}$ and $\text{O2}\cdots\text{O23}$ distances of 2.713(3) and 2.801(3) Å, respectively]. The dimers were stacked together through offset, face-to-face π - π -stacking interactions, which alternated between the central pym ring and the N8 and N1 containing py rings. The centroid-centroid distances for these two π - π -stacking interactions were 3.70 and 3.62 Å, respectively. As a result of these interactions, the dimers were linked together to form a diagonal one-dimensional chain in the $[101]$ direction (Figure 6).

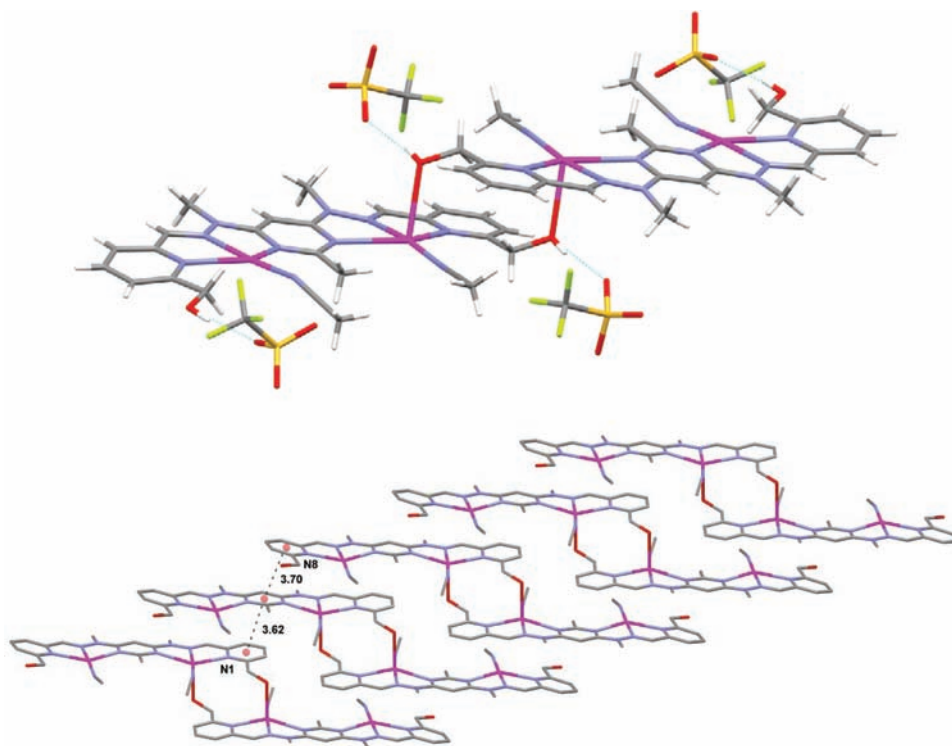


Figure 6. (top) View of complex 2. The two $[\text{Ag}_2\text{I}(\text{CH}_3\text{CN})_2]^{2+}$ cations were bridged by self-complementary coordination bonds between O1 and Ag1. (bottom) View of the arrangement of 2 into a one-dimensional chain through π - π -stacking interactions between the pym and py rings (anions and H atoms are removed for clarity; distances are given in Å).

X-ray Crystal Structure of 3. Crystals of complex 3 were obtained through the slow diffusion of diethyl ether into a CH_3CN solution of AgSO_3CF_3 and 1 in a 1:1 metal-to-ligand ratio. Complex 3 crystallized in the monoclinic space group $C2/c$ with one $[\text{Ag}_2\text{I}(\text{SO}_3\text{CF}_3)(\text{CH}_3\text{CN})_2]^+$ cation, an unbound SO_3CF_3^- counterion, and a H_2O molecule of crystallization in the asymmetric unit. Both pym-hyz bonds in the cation adopted a cisoid conformation, resulting in a linear complex with a distance between the centroids of the terminal py rings of 13.75 Å. The large ellipsoids of the N8-containing py ring indicated considerable ring flexing. This motion appeared to be inherent in the structure because it was present in all of the structure solutions derived from multiple X-ray data collections on crystals of this compound.

The geometry around Ag1 was that of a distorted square pyramid ($\tau_5 = 0.20$),²³ with coordination bonds between Ag1 and the three N donors of a pym-hyz-py site, a CH_3CN molecule, and the hydroxymethyl donor O1 of a symmetry-generated $[\text{Ag}_2\text{I}(\text{SO}_3\text{CF}_3)(\text{CH}_3\text{CN})_2]^+$ cation (Figure 7). This self-complementary Ag1-O1A bond linked adjacent $[\text{Ag}_2\text{I}(\text{SO}_3\text{CF}_3)(\text{CH}_3\text{CN})_2]^+$ cations together as a dimer (Figure 8). The distance of this bond was 2.461(5) Å. The geometry around Ag2 was variable because of the O11-containing SO_3CF_3^- being disordered by translation over two sites, of which only one involved coordination to Ag2. The geometry with O11 bound to Ag2 in an axial position (site occupancy factor 0.33) was that of a distorted five-coordinate square pyramid with a τ_5 parameter of 0.07.²³ The geometry when O11 was not bound (site occupancy factor 0.67) was that of a distorted tetrahedron with a τ_4 parameter of 0.62 (Figure 7).²⁵

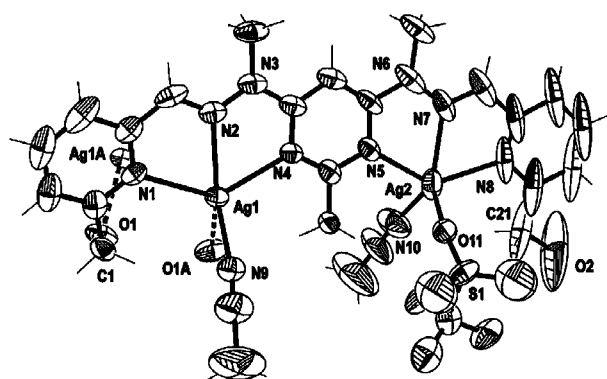


Figure 7. View of the $[\text{Ag}_2\text{I}(\text{SO}_3\text{CF}_3)(\text{CH}_3\text{CN})_2]^+$ cation, which accounted for half of the dimeric complex **3** (crystallographic numbering). Thermal ellipsoids drawn at the 50% probability level (symmetry code: A, $2 - x, y, 5/2 - z$).

Unlike complex **2**, the cations in complex **3** were oriented on top of each other, with the pym methyl groups on each cation pointing in the same direction. There was a face-to-face π - π -stacking interaction between the N1-containing py ring on one cation and the pym ring on the other cation of the dimer (centroid-centroid distance 3.80 Å; Figure 8). A face-to-face π - π -stacking interaction between the N8-containing py rings on adjacent dimers (centroid-centroid distance of 3.90 Å) organized the dimers into an infinite one-dimensional chain that ran in the diagonal [101] direction (Figure 8). No other intermolecular interactions could be determined because of the highly disordered nature of the SO_3CF_3^- counteranions.

X-ray Crystal Structure of 4. Crystals of complex **4** were obtained through the slow diffusion of diethyl ether into a 1:2 mixture of CH_3CN and CH_3NO_2 containing AgSO_3CF_3 and **1** in a 1:1 metal-to-ligand ratio. Complex **4** crystallized in the orthorhombic space group $Pbcn$, with one $[\text{Ag}_2\text{I}_2]^{2+}$ cation, two SO_3CF_3^- counterions, and three CH_3NO_2 molecules of crystallization. The $[\text{Ag}_2\text{I}_2]^{2+}$ cation existed as a double helicate, with two molecules of **1** sharing two Ag^{I} ions (Figure 9). The pym-hyz bonds of both molecules of **1** remained in a

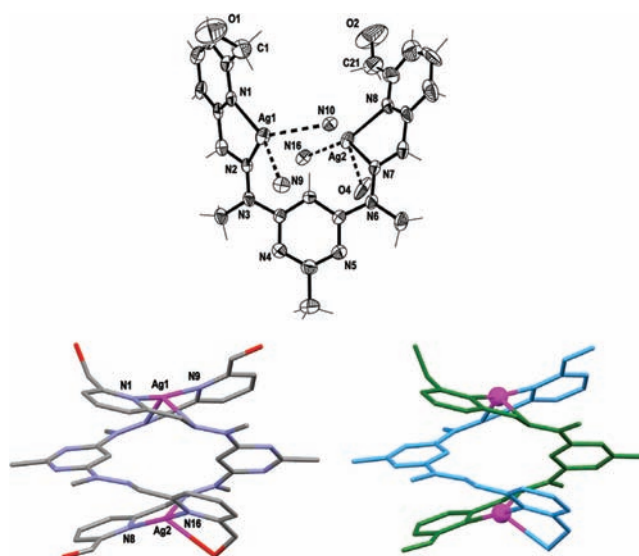


Figure 9. (top) View of one of the arms of the double-helicate $[\text{Ag}_2\text{I}_2]^{2+}$ cation of complex **4** (crystallographic numbering). Thermal ellipsoids drawn at the 50% probability level. (bottom left) View of complex **4** along the c axis. (bottom right) Representation of the double-helicate $[\text{Ag}_2\text{I}_2]^{2+}$ cation of complex **4** with the molecules of **1** color-coded (H atoms are omitted for clarity).

transoid conformation as a result of each Ag^{I} ion being bound to the hyz and py N donors of both molecules of **1** but not the pym N donors of the pym-hyz-py coordination pockets (Figure 9). $\text{Ag}1$ existed in a heavily distorted tetrahedral geometry ($\tau_4 = 0.51$),²⁵ bound to only the hyz and py N donors of both molecules of **1**. The geometry of $\text{Ag}2$ was also a heavily distorted tetrahedron (τ_4 parameter equal to 0.51);²⁵ however, it was bound to the hyz and py N donors of one molecule of **1**, and the hydroxymethyl arm and py N donor of the other molecule of **1**. As a result, the double helicate was not symmetrical, unlike the double helicate identified by NMR spectroscopy. The distance from $\text{Ag}2$ to the unbound hyz N donor (N15) was 2.747(5) Å, which was too long to be

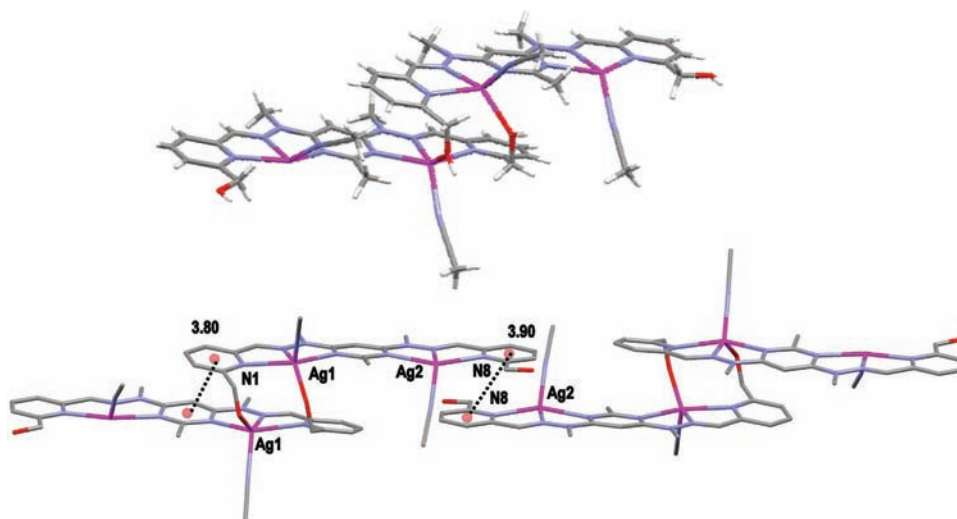


Figure 8. (top) View of complex **3**. The two $[\text{Ag}_2\text{I}(\text{SO}_3\text{CF}_3)(\text{CH}_3\text{CN})_2]^+$ cations were bridged by the self-complementary $\text{Ag}1\text{-O}1$ coordination bonds (the bound SO_3CF_3^- anion has been removed for clarity). (bottom) View of the arrangement of **3** into a one-dimensional chain in the [101] direction through π - π -stacking interactions between the N8-containing py rings. The π - π -stacking interaction between the N1-containing py ring and the pym ring is also shown (the bound SO_3CF_3^- anions are removed for clarity; distances are given in Å).

considered a coordination bond. The Ag–Ag distance across the helicate was 5.09 Å.

A hydrogen bond existed between O11 of one of the SO_3CF_3^- counterions and the major position of O2 (site occupancy factor 0.67) on the helicate. The O2–H...O11 distance was 2.07(2) Å, which corresponded to a O2...O11 distance of 2.89(2) Å. There was a weak π – π interaction between the pym ring containing N4 on one molecule of **1** of the double helicate and the py ring containing N9 on the other molecule of **1** on the double helicate (centroid–centroid distance of 3.74 Å). This interaction may have helped to stabilize the double-helicate structure.

X-ray Crystal Structure of 5. Crystals of complex **5** were obtained through the slow diffusion of diethyl ether into the CH_3CN solution of AgBF_4 and **1** in a metal-to-ligand ratio of 4:1. The structure was refined as a racemic twin.²² Complex **5** crystallized in the triclinic space group $P1$, with one $[\text{Ag}_2\text{I}(\text{CH}_3\text{CN})_2]^{2+}$ cation and two BF_4^- anions in the asymmetric unit (Figure 10). The complex had a linear

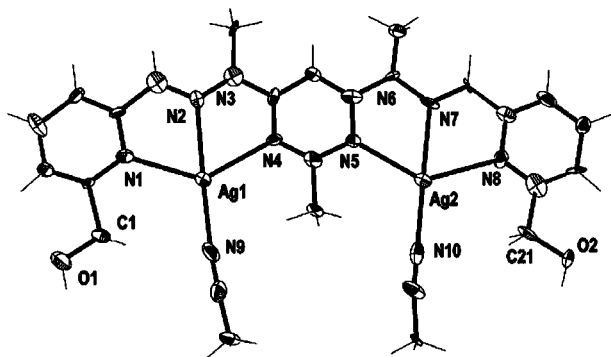


Figure 10. View of the $[\text{Ag}_2\text{I}(\text{CH}_3\text{CN})_2]^{2+}$ cation of complex **5** (crystallographic numbering). Thermal ellipsoids drawn at the 50% probability level.

shape, with cisoid pym–hyz bonds and a distance of 13.85 Å between the centroids of the terminal py rings. There was a Ag^{I} ion in both pym–hyz–py coordination pockets, each of which were bound to all three N donors and a CH_3CN molecule. Both Ag1 and Ag2 existed in a distorted square-planar geometry, with τ_4 parameters of 0.35 and 0.37, respectively.²⁵

Unlike complexes **2** and **3**, complex **5** existed as a discrete molecule. The hydroxymethyl arms were oriented away from the Ag^{I} ions, and there were no significant interactions between adjacent molecules of **5** or between **5** and the two BF_4^- counterions (Figure 10).

X-ray Crystal Structure of 6. Crystals of complex **6** were obtained through the slow diffusion of diethyl ether into a CH_3NO_2 solution of AgBF_4 and **1** in a 1:1 metal-to-ligand ratio. Complex **6** crystallized in the monoclinic space group $P2_1/n$, with one $[\text{Ag}_2\text{I}_2]^{2+}$ cation, two BF_4^- counterions, and two CH_3NO_2 molecules of crystallization. The $[\text{Ag}_2\text{I}_2]^{2+}$ cation existed as a double helicate, with two molecules of **1** sharing two Ag^{I} ions (Figure 11). The conformation of the molecules of **1** in complex **6** was very similar to that seen in complex **4**, with all hyz bonds in a transoid conformation and all of the terminal py rings rotated (Figure 11). The double helicate was also asymmetric, unlike the AgBF_4 double helicate identified in solution by NMR spectroscopy. Ag1 was bound to the py and hyz N donors of both molecules of **1** and the hydroxymethyl arm of one of the molecules of **1**, giving Ag1 a distorted

trigonal-bipyramidal geometry, with a τ_5 parameter of 0.88.²³ Ag2 was disordered over two sites. In the major position (occupancy factor 0.80), Ag2 was bound to the py N atom and hydroxymethyl arm on one molecule of **1** and the py and hydrazine N atoms of the other molecule of **1** in a very distorted tetrahedral geometry (τ_4 of 0.52).²⁵ The distance from Ag2 to the unbound hydrazine N atom was 2.77 Å. The Ag–Ag distance in the helicate was 5.31 Å.

There was a weak π – π -stacking interaction between the N8-containing py ring on one of the molecules **1** and the pym ring on the other molecule of **1** (centroid–centroid distance of 3.68 Å), which may have helped stabilize the double-helicate structure. The double helicate existed as a discrete unit, with no significant intermolecular interactions with the BF_4^- counterions, CH_3NO_2 solvent molecules, or adjacent double helicates.

Comparison of Metal Complex X-ray Structures. The variance in the primary structure seen among complexes **2**–**6** demonstrates the sensitivity of the silver(I) complexes of ligand **1** to changes in the metal-to-ligand ratio, counteranion, and solvent. Complex **2** crystallized from a CH_3CN solution of AgSO_3CF_3 and **1** in a 5:1 metal-to-ligand ratio as a dimer due to self-complementary coordination between one of the hydroxymethyl arms and one of the Ag^{I} ions on adjacent $[\text{Ag}_2\text{I}(\text{CH}_3\text{CN})_2]^{2+}$ cations. This coordination was not witnessed in complex **5**, which was crystallized from a CH_3CN solution of AgBF_4 and **1** in a 4:1 metal-to-ligand ratio, the structure of which was a simple discrete linear complex with no significant intermolecular interactions. Neither complex **2** nor **5** showed any coordination of the SO_3CF_3^- or BF_4^- counterions to Ag^{I} because the coordination sphere of each of the Ag^{I} ions in both complexes was completed by a CH_3CN molecule. However, despite the lack of direct involvement of the counteranions with coordination of the Ag^{I} ions, complexes **2** and **5** had such remarkably different structures.

The impact of using a coordinating solvent such as CH_3CN as opposed to a noncoordinating solvent such as CH_3NO_2 is apparent when comparing complexes **3**, **4**, and **6**. Complex **3** was an attempt to crystallize the double-helicate complex identified by NMR spectroscopy as the exclusive complex in the CH_3CN solution of AgSO_3CF_3 and **1** in a 1:1 metal-to-ligand ratio. Instead, the isolated crystals were that of complex **3**, which was an isomer of the dimeric complex **2**. We hypothesize that during crystallization the double helicate, identified in solution by ^1H NMR spectroscopy, opened up at one end to form a V-shaped complex containing two molecules of **1** sharing one Ag^{I} ion at the pivot. Ag^{I} ions were exchanged between neighboring V-shaped complexes to fill the now empty coordination sites of the complexes, resulting in rotation of the hyz linkages in **1** from transoid to cisoid. This resulted in the formation of the dimeric structure of complex **3** (Figure 12).

Complex **4**, on the other hand, was crystallized from a solution containing AgSO_3CF_3 and **1** in a 1:1 metal-to-ligand ratio dissolved in CH_3NO_2 and CH_3CN in a 2:1 ratio, in an attempt to limit coordination of CH_3CN in the crystallized complex. The structure of complex **4** was a double helicate, similar in form to the complex identified in solution by ^1H NMR spectroscopy. Complex **4** did not contain any CH_3CN molecules, and the Ag^{I} ions were bound only to the N and O donors of the pym–hyz–py coordination pockets of **1**. Likewise, the double-helicate-shaped complex **6** was crystallized from a CH_3NO_2 solution, this time containing AgBF_4 and **1** in

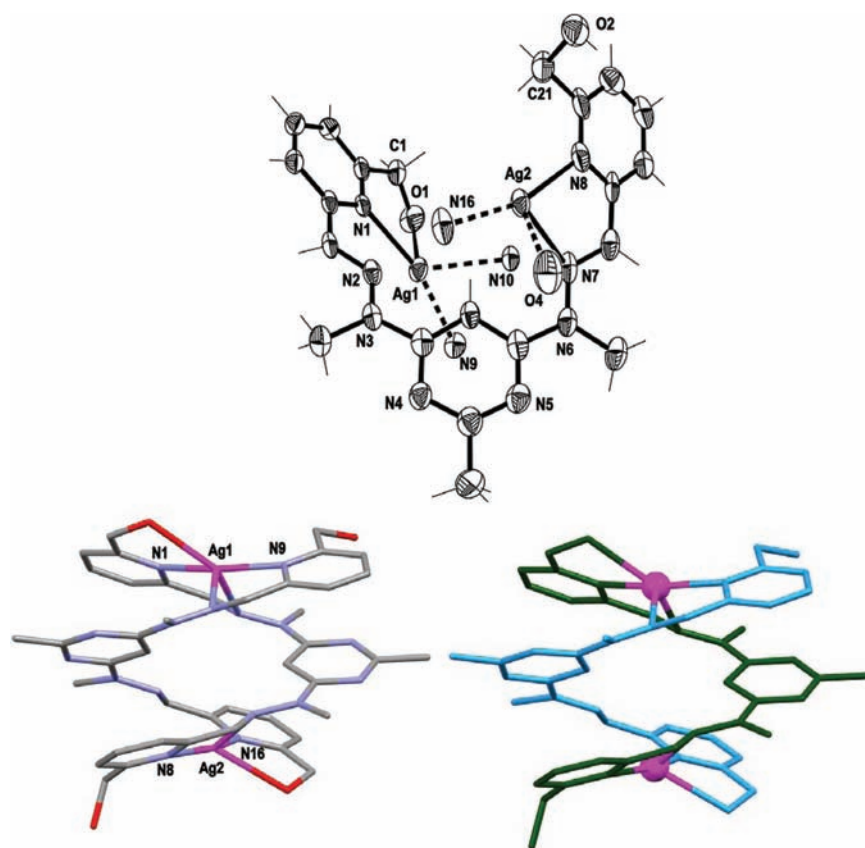


Figure 11. (top) View of one of the arms of the double-helicate $[\text{Ag}_2\text{I}_2]^{2+}$ cation of complex **6** (crystallographic numbering). Thermal ellipsoids drawn at the 50% probability level. (bottom left) View of complex **6** along the c axis. (bottom right) Representation of the double-helicate $[\text{Ag}_2\text{I}_2]^{2+}$ cation of complex **6** with the molecules of **1** color coded (H atoms are omitted for clarity).

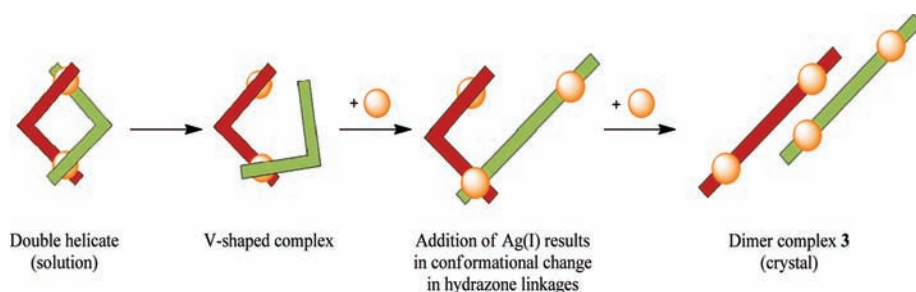


Figure 12. Proposed mechanism for the structural change that occurs during crystallization of the 1:1 AgSO_3CF_3 and **1** complex in CH_3CN , from the double-helicate complex identified in solution to the 2:1 dimeric complex **3**.

a 1:1 metal-to-ligand ratio. It also did not show any interactions between the Ag^{I} ions and the CH_3NO_2 solvent molecules. Complex **3**, on the other hand, had one CH_3CN molecule coordinated to each of its Ag^{I} ions. It, therefore, appears that the coordinating nature of the CH_3CN solvent resulted in the conformational change from double helicate to dimer during crystallization.

The choice of solvent and counteranion also affected the conversion of the double helicate to the linear complex in solution, as evidenced by NMR spectroscopy. In CD_3CN , total conversion of the AgSO_3CF_3 double helicate to the linear complex required a 7:1 metal-to-ligand ratio. This is significantly lower than the 12:1 metal-to-ligand ratio required to convert 85% of the AgBF_4 double helicate of a previous *pym-hyz* ligand without hydroxymethyl arms to the linear complex.⁷ In CD_3NO_2 , however, the AgSO_3CF_3 double-helicate

complex showed no conversion to the linear complex, even at metal-to-ligand ratios of 8:1. Likewise, reacting AgBF_4 and **1** in CH_3NO_2 only resulted in the formation of the double helicate, regardless of the metal-to-ligand ratio used. However, reacting AgBF_4 and **1** in CH_3CN did show minor conversion of the double helicate to the linear complex, though the double helicate was always a major product even at high metal-to-ligand ratios.

CONCLUSION

The reactions of AgSO_3CF_3 and AgBF_4 with ligand **1** in CH_3CN or CH_3NO_2 resulted in a variety of complex structures that were influenced greatly by the counteranion, solvent, and metal-to-ligand ratio used. NMR spectroscopy showed that both silver(I) salts in either solvent produced a double-helicate complex in solution when a 1:1 metal-to-ligand ratio was

employed. As the metal-to-ligand ratio was increased, conversion of this double-helicate complex to a linear complex was witnessed; however, total conversion to the linear complex was only achievable with AgSO_3CF_3 in CH_3CN , with a required metal-to-ligand ratio of 7:1.

X-ray diffraction performed on the crystals grown from the various reaction solutions showed that the solid-state structure of the silver(I) complexes of **1** were often different from those seen in solution. Crystals grown from the CH_3CN solution of AgSO_3CF_3 and **1** in a 5:1 metal-to-ligand ratio contained a complex dimer, instead of the discrete linear complex observed in solution by NMR spectroscopy. However, crystals grown from the analogous CH_3CN solution of AgBF_4 and **1** showed a discrete linear complex, which did match the NMR spectra.

Attempts to crystallize the AgSO_3CF_3 and **1** double-helicate complex from a CH_3CN solution resulted in another dimeric complex, while crystals grown from a mixture of CH_3CN and CH_3NO_2 gave a double-helicate structure similar in form to the complex identified in solution by NMR spectroscopy. A double-helicate complex was also crystallized from a CH_3NO_2 solution of AgBF_4 and **1** in a 1:1 metal-to-ligand ratio. The noncoordinating nature of the CH_3NO_2 solvent appeared to promote the retention of the double-helicate structure during crystallization, as opposed to the CH_3CN solvent, which coordinated to the Ag^{I} ions during crystallization, resulting in the formation of the dimeric complex.

The addition of the hydroxymethyl arms to the terminal py rings of **1** has therefore resulted in a greater complexity in the silver(I) chemistry of simple pym-hyz ligands. Coordination of the hydroxymethyl arms to the Ag^{I} ions resulted in the dimeric complexes seen in the solid state. The solid-state and solution structures of the double-helicate complexes also showed coordination of the arms to the Ag^{I} ions, however, unlike in the case with Cu^{II} ions, the flexible Ag^{I} coordination sphere was able to accommodate their presence in addition to two molecules of **1**.

■ ASSOCIATED CONTENT

Supporting Information

X-ray crystallographic data in CIF format and a table of selected bond lengths and angles for complexes **2**–**6**. This material is available free of charge via the Internet at <http://pubs.acs.org>.

■ AUTHOR INFORMATION

Corresponding Author

*E-mail: lhanton@chemistry.otago.ac.nz. Phone: (+64) 3-479-7918. Fax: (+64) 3-479-7906.

Notes

The authors declare no competing financial interest.

■ ACKNOWLEDGMENTS

We thank the Department of Chemistry, University of Otago, and the New Economic Research Fund of the Foundation for Research, Science and Technology (NERF Grant UOO-X0808) for financial support.

■ REFERENCES

(1) Young, A. G.; Hanton, L. R. *Coord. Chem. Rev.* **2008**, *252*, 1346–1386.
 (2) (a) Duong, A.; Métivaud, V.; Maris, T.; Wuest, J. D. *Cryst. Growth Des.* **2011**, *11*, 2026–2034. (b) Lusby, P. J. *Annu. Rep. Prog. Chem., Sect. A* **2009**, *105*, 323–347.

(3) (a) Li, C.-P.; Wu, J.-M.; Du, M. *Inorg. Chem.* **2011**, *50*, 9284–9289. (b) Wenzel, M.; Wichmann, K.; Gloe, K.; Gloe, K.; Buschmann, H.-J.; Otho, K.; Schröder, M.; Blake, A. J.; Wilson, C.; Mills, A. M.; Lindoy, L. F.; Plieger, P. *CrystEngComm* **2010**, *12*, 4176–4183. (c) Steel, P. J.; Fitchett, C. M. *Coord. Chem. Rev.* **2008**, *252*, 990–1006. (d) Bu, X.; Chen, W.; Hou, W.-F.; Du, M.; Zhang, R.-H.; Brisse, F. *Inorg. Chem.* **2002**, *41*, 3477–3482.

(4) (a) Wimberg, J.; Scheele, U. J.; Dechert, S.; Meyer, F. *Eur. J. Inorg. Chem.* **2011**, 3340–3348. (b) Wu, C.-J.; Lin, C.-Y.; Cheng, P.-C.; Yeh, C.-W.; Chen, J.-D.; Wang, J.-C. *Polyhedron* **2011**, 2260–2267.

(5) (a) Wu, C.-J.; Sie, M.-J.; Hsiao, H.-L.; Chen, J.-D. *CrystEngComm* **2011**, *13*, 4121–4130. (b) Du, M.; Li, C.-P.; Guo, J.-H. *CrystEngComm* **2009**, *11*, 1536–1540. (c) Niu, C.-Y.; Wu, B.-L.; Zheng, X.-F.; Wan, X.-S.; Zhang, H.-Y.; Nui, Y.-Y.; Meng, L.-Y. *CrystEngComm* **2009**, *11*, 1373–1382. (d) Reger, D. L.; Watson, R. P.; Gardinier, J. R.; Smith, M. D. *Inorg. Chem.* **2004**, *43*, 6609–6619.

(6) (a) Chakraborty, B.; Halder, P.; Paine, T. K. *Dalton Trans.* **2011**, 40, 3647–3654. (b) Li, C.-P.; Du, M. *Chem. Commun.* **2011**, 47, 5958–5972. (c) Amoores, J. J. M.; Black, C. A.; Hanton, L. R.; Spicer, M. D. *Cryst. Growth Des.* **2005**, *5* (3), 1255–1261. (d) Blake, A. J.; Champness, N. R.; Hubberstey, P.; Li, W.-S.; Withersky, M. A.; Schröder, M. *Coord. Chem. Rev.* **1999**, *183*, 117–138.

(7) Stadler, A.-M.; Kyritsakas, N.; Vaughan, G.; Lehn, J.-M. *Chem.—Eur. J.* **2007**, *13*, 59–68.

(8) (a) Chaur, M.; Collado, D.; Lehn, J.-M. *Chem.—Eur. J.* **2011**, *17*, 248–258. (b) Schmitt, J.-L.; Stadler, A.-M.; Kyritsakas, N.; Lehn, J.-M. *Helv. Chim. Acta* **2003**, *86*, 1598–1624. (c) Gardinier, K. M.; Khoury, R. G.; Lehn, J.-M. *Chem.—Eur. J.* **2000**, *6* (22), 4124–4131.

(9) Stadler, A.-M.; Kyritsakas, N.; Graff, R.; Lehn, J.-M. *Chem.—Eur. J.* **2006**, *12*, 4503–4522.

(10) (a) Cao, X.-Y.; Harrowfield, J.; Nitschke, J.; Ramirez, J.; Stadler, A.-M.; Kyritsakas-Gruber, N.; Madalan, A.; Rissanen, K.; Russo, L.; Vaughan, G.; Lehn, J.-M. *Inorg. Chem.* **2007**, 2944–2965. (b) Ramirez, J.; Stadler, A.-M.; Harrowfield, J. M.; Brelot, L.; Huuskonen, J.; Rissanen, K.; Allouche, L.; Lehn, J.-M. *Z. Anorg. Allg. Chem.* **2007**, 633, 2435–2444. (c) Giuseppone, N.; Schmitt, J.-L.; Lehn, J.-M. *J. Am. Chem. Soc.* **2006**, *128*, 16748–16763. (d) Tielmann, P.; Marchal, A.; Lehn, J.-M. *Tetrahedron Lett.* **2005**, *46*, 6349–6353.

(11) Hutchinson, D. J.; Hanton, L. R.; Moratti, S. C. *Inorg. Chem.* **2010**, *49*, 5923–5934.

(12) (a) Maeda, S.; Hara, Y.; Nakamaru, S.; Hashimoto, S. *Polymers* **2011**, *3*, 299–313. (b) Lee, K. S.; Jeon, B. J.; Cha, S. W. *Smart Mater. Struct.* **2010**, *19*, 065029–065036. (c) Schneider, H.-J.; Strongin, R. M. *Acc. Chem. Res.* **2009**, *42* (10), 1489–1500. (d) Huck, W. T. S. *Mater. Today* **2008**, *11* (7), 24–32. (e) Kay, E. R.; Leigh, D. A.; Zerbetto, F. *Angew. Chem., Int. Ed.* **2007**, *46*, 72–191. (f) Balzani, V.; Credi, A.; Raymo, F. M.; Stoddart, J. F. *Angew. Chem., Int. Ed.* **2000**, *39*, 3348–3391.

(13) Hutchinson, D. J.; Hanton, L. R.; Moratti, S. C. *Inorg. Chem.* **2011**, *50*, 7637–7649.

(14) (a) Otwinowski, Z.; Minor, W. Processing of X-Ray Diffraction Data Collected in Oscillation Mode. In *Methods in Enzymology*; Carter, C. W., Jr., Sweet, R. M., Eds.; Academic Press: New York, 1997; Vol. 276, pp 307–326. (b) SAINT V4, Area Detector Control and Integration Software; Siemens Analytical X-Ray Systems Inc.: Madison, WI, 1996.

(15) Sheldrick, G. M. SADABS, Program for Absorption Correction; University of Göttingen: Göttingen, Germany, 1996.

(16) Sheldrick, G. M. *Acta Crystallogr., Sect. A* **1990**, *46*, 467–473.

(17) Altomare, A.; Burla, M. C.; Camalli, M.; Cascarano, G. L.; Giacovazzo, C.; Guagliardi, A.; Moliterni, A. G. G.; Polidori, G.; Spagna, R. *J. Appl. Crystallogr.* **1999**, *32*, 115–119.

(18) Sheldrick, G. M. SHELXL-97, Program for the Solution of Crystal Structures; University of Göttingen: Göttingen, Germany, 1997.

(19) Farrugia, L. J. *J. Appl. Crystallogr.* **1999**, *32*, 837–838.

(20) Spek, A. L. *Acta Crystallogr., Sect. A* **1990**, *46*, C34.

(21) (a) Macrae, C. F.; Edgington, P. R.; McCabe, P.; Pidcock, E.; Shields, G. P.; Taylor, R.; Towler, M.; van de Streek, J. *J. Appl. Crystallogr.* **2006**, *39*, 453–457. (b) Bruno, I. J.; Cole, J. C.; Edgington,

P. R.; Kessler, M. K.; Macrae, C. F.; McCabe, P.; Pearson, J.; Taylor, R. *Acta Crystallogr., Sect. B* **2002**, *58*, 389–397.

(22) (a) Bernardinelli, G.; Flack, H. D. *Acta Crystallogr., Sect. A* **1985**, *A41*, 500–511. (b) Flack, H. D. *Acta Crystallogr., Sect. A* **1983**, *A39*, 876–881.

(23) Addison, A. W.; Rao, T. N.; Reedijk, J.; van Rijn, J.; Verschoor, G. C. *J. Chem. Soc., Dalton Trans.* **1984**, *7*, 1349–1356.

(24) Hanton, L. R.; Young, A. G. *Cryst. Growth Des.* **2006**, *6*, 833–835.

(25) Yang, L.; Powell, D. R.; Houser, R. P. *Dalton Trans.* **2007**, 955–964.